

Loading and Aging Effects in Exhaust Gas After-Treatment Catalysts with Pt As Active Component

Willi Boll, Steffen Tischer, and Olaf Deutschmann*

Institute for Chemical Technology and Polymer Chemistry, Karlsruhe Institute of Technology (KIT), Engesserstr. 20, 76128 Karlsruhe, Germany

Abatement of pollutant emissions over platinum-containing catalytic converters of lean operated engines is studied. Several close-to-production model catalysts with varying platinum loading and hydrothermal aging procedures are characterized by BET, HR-SEM, HR-TEM, and CO-TPD. Pollutant conversion is numerically investigated in an isothermal flat bed reactor using varying lean exhaust-gas mixtures and temperatures. The performance of the monolithic catalysts is modeled by a two-dimensional flow field description of a single channel coupled with models for washcoat diffusion and multistep reaction mechanisms. An optimizing procedure is presented which allows adaption of kinetic parameters for slightly different catalysts. The catalytic active surface area of the catalyst determined by CO-TPD can serve as parameter to model the varying noble metal loading and consequences of hydrothermal aging without any adaption of the kinetic data included in the reaction mechanism.

1. Introduction

In spite of the enormous achievements in the after-treatment of exhaust-gas emissions, the increasing number of vehicles worldwide represents a serious environmental problem due to vehicles' raw emissions, in particular carbon dioxide, which has a strong impact on the greenhouse effect. A more efficient fuel consumption can be achieved by diesel and lean operated engines. Here, the problem is the abatement of nitrogen oxides (NO_x). Since improvements of the combustion process itself are not sufficient to meet future legislative limits, the development of a technique for the after-treatment of NO_x is urgently needed.

For passenger cars and light duty applications, the NO_x-Storage Catalyst (NSC)^{1,2} which utilizes the NO_x storage on barium sites to form nitrates during the lean phase and their reduction to nitrogen in a rich atmosphere is a very promising approach. Detailed models^{3,4} based on physical and chemical processes on the molecular level are indispensable to exploit the full potential of this technique. However, catalysts consist of several components with different promoting and storage functionalities which show complex interactions among themselves. Therefore, as a first step toward a complete NSC model, the noble metal activity of NSCs is considered. Such a catalytic system is realized in a diesel oxidation catalyst (DOC), consisting of a single platinum component. Particularly with regard to the limited thermal stability of the NSC, it is fundamental that the effect of aging is taken into account.

In this work an approach is evaluated according to which the catalytic active platinum surface can be directly related to the conversion rates of all pollutants for catalysts with varying noble metal loadings and aging procedures. This enables accurate prediction for pollutant conversion for DOCs and subsequently NSCs with different platinum loading and aging state only by determining the catalytic active surface area by CO-TPD. To set up a broad basis for model development, several close-to-production catalysts with a specified platinum loading were hydrothermally aged and subsequently characterized. For simulation of the catalyst behavior at work, a two-

dimensional flow field description of a single channel of the monolithic structure coupled with models for washcoat diffusion and multistep reaction mechanisms was applied and compared with experimental results.

2. Experiments

2.1. Catalyst Conditioning and Aging. Monolithic samples with different platinum loading have been manufactured in a close-to-production procedure by a commercial catalyst supplier and were conditioned with 10% water in air for 16 h at 700 °C. In addition, fresh samples with the very high loading were hydrothermally aged with 10% water in air for 16 h at elevated temperatures. All pretreatment steps were conducted in an oven with no flow. For comparability, sample DOC120 (shown in Table 1) serves as reference for coupling both noble metal variation and hydrothermal aging.

2.2. Characterization Techniques. The catalysts were characterized by several chemical and physical methods such as light and electron microscopy, BET surface area, and CO-TPD to evaluate crucial parameters for the reactor model and to identify changes in the catalyst properties due to variation in noble metal loading and hydrothermal aging.

The specific surface areas of the conditioned and aged catalysts were determined by the BET method after nitrogen adsorption in a micropore analyzer (Belsorp Mini 2). Before adsorption, the washcoat of all samples was removed mechanically from the substrate and was pretreated in vacuum at 300 °C for 2 h.

Light microscopy (Leica Reichert MRF4M) was used to measure geometric parameters of the coated channels. Therefore, monolithic samples of the catalysts were embedded in epoxy resin and polished with diamond paste for improved imaging. For the investigation of the nanoscale platinum particles and

Table 1. Model Catalysts

sample name	platinum metal loading [g/ft ³]	conditioning/aging temperature [°C]
DOC20	22.51	700
DOC60	58.37	700
DOC120	130.06	700
DOC120-850	127.80	850
DOC120-950	129.97	950

* To whom correspondence should be addressed. E-mail: deutschmann@kit.edu. Tel: +49 721 608 3064. Fax: +49 721 608 4805u.

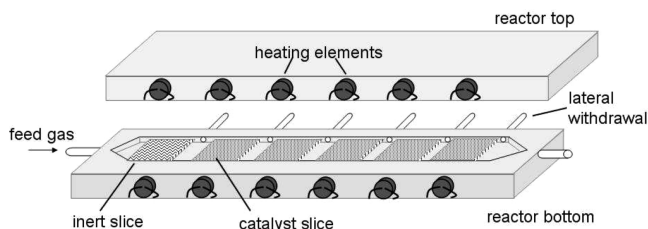


Figure 1. Sketch of the isothermal flat bed reactor.⁶

washcoat structure, high-resolution electron microscopy (HR-SEM: Leo 1530 Gemini, HR-TEM: Philips CM200 FEG) combined with energy dispersive X-ray spectroscopy (EDX) for component identification was consulted. For sample preparation, washcoat powder was suspended in acetone and small washcoat particles were superimposed on a copper net enmeshed with carbon fibers by an ultrasonic fumigation procedure. The platinum particle size distribution was obtained by analysis of HR-TEM images using several hundred particles for evaluation.

To determine the catalytic active surface, CO-TPDs⁵ were carried out in a quartz tube flow reactor with an in situ thermal conductivity detector (TCD; Shimadzu GC-14B) for gas analysis. Before adsorption, the monolithic samples were pretreated at 400 °C with 10% H₂ in helium for 16 h for complete platinum reduction. After purging the sample for 30 min in pure helium, the temperature was set to 25 °C and the catalyst was saturated with 10% CO in helium for 30 min and purged for additional 30 min. The temperature was annealed to 500 °C with a rate of 30 °C/min. The noble metal dispersion was calculated by integration of TCD signal assuming stoichiometric adsorption of CO on platinum.

2.3. Kinetic Measurements. Small slices of monolith catalysts (400 cpsi) have been studied under realistic flow conditions (SV = 40,000 h⁻¹) with synthetic exhaust gas. The experiments were carried out in an isothermal flat bed reactor⁶ at ICVT, University of Stuttgart, shown in Figure 1. Five thin catalyst slices (30 mm × 40 mm, one channel height) were placed behind one inert slice for gas preheating and ensuring uniform inlet flow distribution. Lateral withdrawals after each slice allowed the measurement of gas concentration profiles along the flow direction. Gas analysis was conducted with SI-mass spectroscopy (MS4). Lean steady-state experiments with concentration variations of single gas components as well as complex gas mixtures were investigated. The temperature was varied between 120 and 450 °C.

3. Mathematical and Numerical Model

3.1. Modeling the Channel Flow. In the experiment, all channels in a catalyst slice behave essentially alike and therefore, the analysis of a single channel model only is sufficient to understand the catalyst behavior. The DETCHEM^{CHANNEL} code⁷ is applied to compute the steady state two-dimensional flow field in a cylindrical channel using the boundary-layer assumption. This assumption is suitable for systems with a main direction of the convective flow, in which the diffusive transport along this direction is negligible. This becomes valid for a channel with sufficiently high velocity or sufficiently small diameter of the channel and is well-suited for all catalysts used in this study. Radial transport models include composition- and temperature-dependent transport coefficients in the gas phase and an effectiveness factor approach for diffusion and reaction in the washcoat. The species properties are based on atomistic models and reactions among gas-phase, and surface species based on elementary-step like reaction mechanisms are included

in the model. Because the temperature range considered never exceeds 450 °C, gas-phase reactions in the fluid flow can be neglected.

The model approach leads to the following conservation equations for a single isothermal channel:

Continuity equation

$$\frac{\partial(\rho u)}{\partial z} + \frac{1}{r} \frac{\partial(r\rho v)}{\partial r} = 0$$

Axial momentum

$$\rho u \frac{\partial u}{\partial z} + \rho v \frac{\partial u}{\partial r} = -\frac{\partial p}{\partial z} + \frac{1}{r} \frac{\partial}{\partial r} \left(\mu r \frac{\partial u}{\partial r} \right)$$

Radial momentum

$$0 = \frac{\partial p}{\partial r}$$

Species continuity

$$\rho u \frac{\partial Y_i}{\partial z} + \rho v \frac{\partial Y_i}{\partial r} = \frac{1}{r} \frac{\partial}{\partial r} (r j_{i,r})$$

Here z and r denote the axial and radial coordinates, respectively, u and v denote their respective velocity components, ρ is density, p is pressure, μ is viscosity, Y_i is mass fractions, and $j_{i,r}$ is diffusive mass fluxes in radial direction. The molar surface reaction rates, \dot{s}_i , are linked to the diffusive mass fluxes by the following boundary condition at the interface of free fluid flow and washcoat:

$$j_{i,r} = \eta \dot{s}_i M_i F_{cat/geo}$$

$F_{cat/geo}$ denotes the ratio between the catalytic surface area of the noble metal and the geometrical area of the cylindrical wall. It can be determined by CO-TPD and serves, in our case, as a parameter to account for both varying loadings and hydrothermal aging. η is the washcoat model effectiveness factor and M_i is molar mass. The viscous transport coefficients and the radial species diffusion fluxes depend on temperature and gas-phase composition. Even though the effectiveness factor model has its limitations if applied in complex reaction systems, the conclusions drawn in the current paper are not affected by this simplification. A more detailed discussion of the impact of diffusion models on catalyst performance in automotive exhaust gas after-treatment can be found in our recent study.⁸

3.2. Surface Reaction Mechanism. Initially, a platinum mechanism,³ consisting of 75 elementary-step like reactions, was applied without any adaption of the kinetic data. It includes dissociative adsorption of O₂, H₂, and nondissociative adsorption of NO, NO₂, N₂O, CO, CO₂, C₃H₆, H₂O, and desorption of all those species. All reactions on platinum are modeled as reversible reactions.

The developed mechanism can be subdivided into four parts:

- the decomposition of hydrocarbons via abstraction of hydrogen atoms,
- the oxidation of carbon monoxide to carbon dioxide,
- the formation of water via an adsorbed hydroxyl species (OH),
- and reactions for the conversion of nitrogen oxides.

The actual exhaust gas composition of a combustion engine typically contains more than 100 different hydrocarbon species and depends on many factors. Because of this complexity, C₃H₆ is commonly chosen as representative HC species for all reactive HCs such as olefins and aromatic hydrocarbons. The oxidation

of propylene proceeds in analogy to the mechanism of Chatterjee et al.⁴ and consists of two reaction pathways. On the one hand, adsorption comes along with abstraction of an H-atom and formation of a propylidene species. After cracking the C–C bond, all remaining carbon atoms are oxidized to CO and CO₂. On the other hand, propylene adsorbs dissociatively on platinum, providing a hydrogen atom that reacts with an adsorbed oxygen atom to form a hydroxyl species. Because elementary details of propylene decomposition are unknown, the remaining oxidation steps are modeled as lumped steps.

Carbon monoxide is converted via a widely accepted Langmuir–Hinshelwood (LH) reaction step,⁹ for which the activation energy also depends on the surface coverage with CO and NO.

In the lean phase, nitrogen oxide is oxidized to nitrogen dioxide, but at temperatures above 350 °C, the conversion is restricted by the thermodynamic equilibrium. The applied mechanism consists of a combination of LH and Eley–Rideal (ER) mechanism for NO oxidation. The forward reaction for LH is highly activated and is additionally limited by increasing surface coverage with carbon monoxide. However, more crucial, the backward reaction is less activated and constitutes an effective source of surface oxygen on platinum, even in an oxygen-rich atmosphere, due to the decomposition of NO₂. The main route for the oxidation of nitrogen oxide is the ER pathway. But more decisive, the oxidation of NO in the ER reaction mechanism is facilitated by high oxygen surface coverage. In a lean gas composition, adsorbed oxygen is the most abundant species which additionally reduces the activation energy of the oxidation.

A qualitative agreement between experimentally measured and numerically predicted conversion was achieved using the recently developed platinum mechanism by Koop et al.³ However, since this mechanism was developed for temperatures above 250 °C and for complex reaction mixtures, its application to predict conversion quantitatively at lower temperatures as considered in the current paper had to be evaluated. Indeed, weaknesses of the mechanism³ were revealed concerning light-off temperatures. Therefore, the values of the kinetic parameters of that previously published mechanism were optimized to match the conducted experiments using the following procedure.

For optimization of the kinetic parameters of the mechanism, experimental data derived of the flat-bed reactor were applied using the catalyst with the highest loading (DOC120). The conversion after the first slice (4 cm) was considered for comparing numerical prediction and experimental measurements. Twenty cases with varying inlet feed compositions and temperatures were selected, for which the conversion after the first slice was significant but not complete. In these cases, the gas composition is most sensitive with respect to the kinetic parameters. For each case, four concentrations were selected as target values of the simulation. Thus, a total of 80 target values (x_i^{exp}) were considered in optimization, trying to minimize the objective function

$$E(\vec{p}) = \sum_i \left(\frac{x_i^{\text{sim}}(\vec{p}) - x_i^{\text{exp}}}{x_i^{\text{ref}}} \right)^2$$

for a set of parameters \vec{p} . Here, x_i^{sim} denotes the results of the numerical simulation and x_i^{ref} is the reference values for normalization (e.g., the inlet feed concentration).

The reaction mechanism itself consists of 129 kinetic parameters (pre-exponential factors, activation energies, and sticking coefficients). Due to thermodynamic constraints, only

20 out of 37 rates of reverse reactions can be chosen independently, i.e., 20 reverse reaction rates are used to define the unknown thermodynamic variables of the 20 surface species. This eliminates 34 dependent kinetic parameters. A procedure of ensuring thermodynamic consistency is presented elsewhere.¹⁰ Thus, 95 parameters can be considered independent. A sensitivity analysis could further reduce the number of significant parameters that need to be optimized. However, in our study all parameters were allowed to change.

A random walk algorithm was applied to minimize the objective function. The parameters were varied independently within the given bounds (activation energies ± 5 kJ/mol, logarithm of pre-exponentials ± 1). To preferably search the vicinity of the current optimum, random step sizes of nearly normal distribution were used. The variance of the Gaussian function was decreased with increasing iteration count. After 1000 iterations with no improvement, a gradient search was applied as final optimization step.

Figure 2 shows a comparison of experimental data with the simulation results before and after optimization. For each of the pollutants, CO, C₃H₆, and NO, a case at light-off temperature and one at higher temperature are shown. During the optimization procedure only the data points in the light-off regime at 4 cm have been used, for which the original kinetic data³ failed to reproduce the spatial profiles of CO and C₃H₆. For these two components a significant improvement of the mechanism was achieved. The spatial profiles match very well over a large temperature range. However, for NO the quality of the mechanism was not improved. As shown for the case of 250 °C, for optimization it was not sufficient to select the data points after the first active slice only. The whole spatial profiles need to be considered.

It has to be noted that parameter fine-tuning can only be applied with great caution. Due to the large number of independent parameters, many more target values would be necessary. However, each parameter can only be varied within a small, physically meaningful range. Thus, the simulation results cannot be pushed into an arbitrary direction to match any (nonsense) data. Of course, the kinetic parameters of the optimized mechanism are not unique, but we are confident that any detailed mechanism would only deviate within narrow bounds. On the other hand, the good agreement of most spatial profiles justified our approach a posteriori, even though we only used a few data for the optimization. This optimization procedure may also be of use for modeling catalysts with varying effects of support and additives on conversion and selectivity by the same reaction mechanism.

4. Results and Discussion

4.1. Washcoat Properties. The influence of hydrothermal aging and noble metal variation on specific surface areas of the model catalysts was determined by nitrogen adsorption (Table 2). The pretreated samples for noble metal variation show a specific surface area of 85 m²/g, except DOC60, for which preparation in a second batch leads to a reduced surface area of 50 m²/g. Taking into account the results from the kinetic measurements, no dramatic change in the conversion behavior is caused by this deviation. After hydrothermal treatment of DOC120, the specific surface area decreases strongly to 72 m²/g and 54 m²/g by increasing the temperature to 850 and 950 °C, respectively.

SEM investigations of the aged catalysts reveal major changes in washcoat morphology. In Figure 3, SEM images of DOC120 (left) and DOC120-950 (right) clarify the loss of washcoat

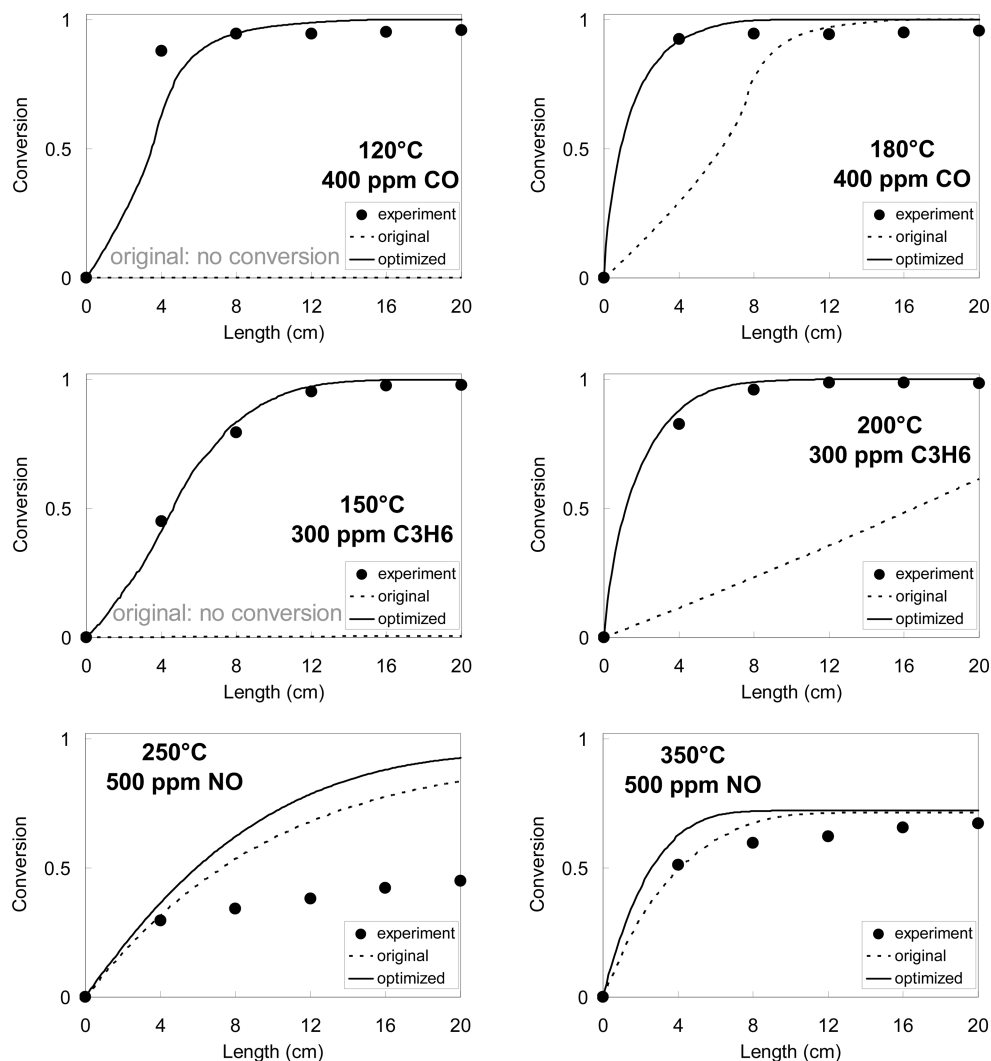


Figure 2. Comparison of experimentally determined profiles with numerically predicted ones with original and optimized parameter sets. Feed gas consists of the component given in the legend and 10% H₂O, 7% CO₂, and 12% O₂, balanced by N₂.

Table 2. Overview of the Specific Surface Area and Pore Radii Distribution

sample name	specific surface area [m ² /g]	maximum pore radii distribution [nm]
DOC20	85	8
DOC60	50	8
DOC120	85	8
DOC120-850	72	8
DOC120-950	54	11

porosity by the formation of a more compact Al₂O₃ structure. This phase transition leads to a more difficult identification of platinum caused by its similar image contrast, and a regular particle analysis by EDX is indispensable.

The maximum of pore radii distribution determined by the Barrett–Joyner–Halenda (BJH) model is neither affected by noble metal variation nor aging temperatures up to 850 °C (Table 2). For the catalyst aged at higher temperature, the maximum is slightly shifted toward higher radii. In principle, all samples exhibit a hysteresis loop of the isotherm (not shown here) that is characteristic for cylindrical pores,¹¹ concluding that hydrothermal aging does not change the shape of the pores in the washcoat. Compared to the narrow pore radii distribution of pure Al₂O₃ around 10 nm¹¹ a bimodal distribution with smaller pore radii is detected for all samples. Because the pore

size and shape are marginal, no parameter adaption in the diffusion model is needed.

4.2. Platinum Particle Size Distribution. The particle size distributions measured by HR-TEM show that the platinum particles of DOC120 are between 15 and 250 nm in diameter (Figure 4). Reduction of the platinum loading leads to a shift in particle size distribution to smaller particles. The smallest particles are found on DOC20 with a diameter of 8 nm. Since DOC60 was prepared in a slightly different procedure, the particle size distribution is narrower.

Hydrothermal aging of DOC120 shows an increase in particle diameter due to sintering of the platinum particles.¹² In addition to the expected increase in particle size for DOC120-850, an increasing number of particles with diameters between 20 and 50 nm which is even higher than for the DOC120, i.e., the non aged catalyst, is also shown in Figure 5. This feature can be understood by Ostwald ripening¹² based on the energetically favored reduction of surface tension. At elevated temperatures, the platinum sinters by atomic migration¹³ toward larger particles on the support surface, leading to a loss of platinum atoms in small particles. As a consequence, DOC120-850 shows the smallest mean particle diameter of the three investigated DOC120 catalysts. At higher aging temperatures (DOC120-950), the migration of atoms is already completed, and all particles are larger than those of DOC120. Hence, the intermediate aged

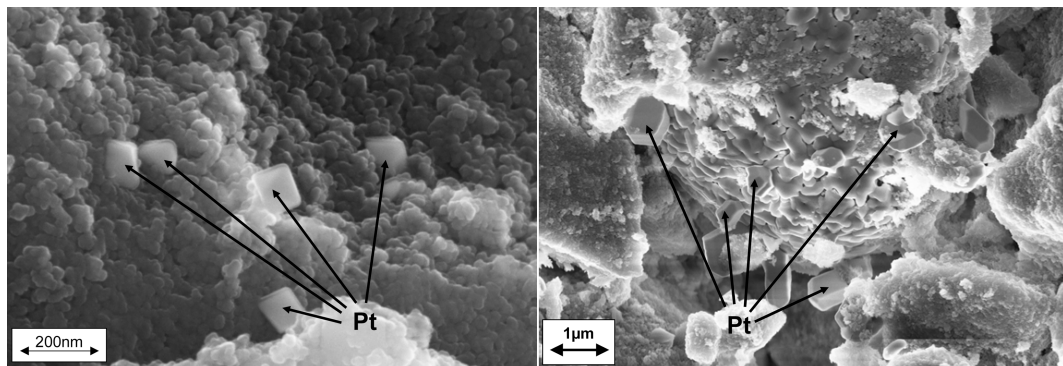


Figure 3. SEM images of the DOC120 (left) and DOC120-950 (right) washcoat structure; note the different scales.

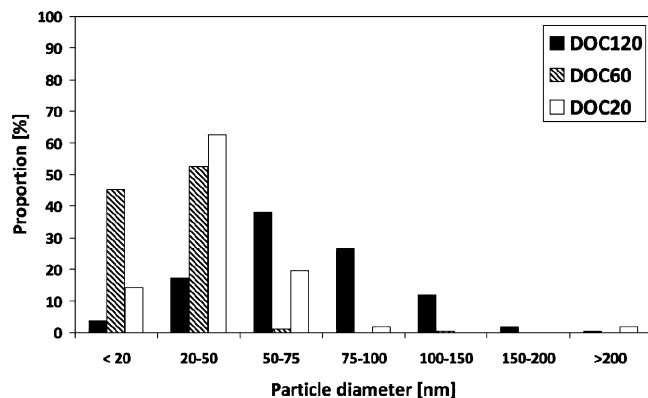


Figure 4. Particle size distribution of catalysts with varying precious metal loading.

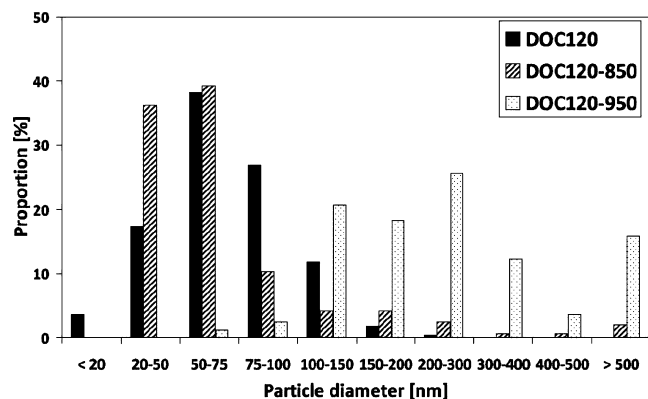


Figure 5. Particle size distribution of catalysts with varying hydrothermal aging temperature.

DOC120-850 can be seen as a snapshot of catalyst aging due to particle sintering.

The variation in particle sizes can lead to a structure sensitivity of the conversion rate, i.e., a varying turnover frequency (TOF) in regard to the number of active sites. The ratio of all active sites (corner, edge, planar face) depends on the particle size, whereas once a critical value is exceeded the ratio hardly changes and the reaction is called structure insensitive. CO oxidation¹⁴ on platinum was shown to be structure sensitive only for 2 nm. All catalysts used in the present study exhibit particle sizes generally larger than 10 nm, i.e., way above this critical size. Thus, particle size dependent effects do not need to be implemented in the model. Consequently, only the total number of active sites is used as parameter to characterize the catalyst activity.

Table 3. Noble Metal Dispersion and Ratio of Catalytic and Geometric Surface Area ($F_{cat/geo}$)

sample name	noble metal dispersion [%]	$F_{cat/geo}$ [-]
DOC20	24.7	19
DOC60	16.2	33
DOC120	10.7	48
DOC120-850	5.6	23
DOC120-950	2.7	11

4.3. Catalytically Active Surface Area. CO-TPDs were used to determine the catalytic active platinum surface for both the catalyst with noble metal variation and the catalysts hydrothermally aged. The ratio between catalytically active and geometrical surface site, $F_{cat/geo}$, serves as model parameter to account for the catalytic activity and is calculated by:

$$F_{cat/geo} = \frac{A_{cat}}{A_{geo}} = \left(D \cdot \frac{m_{cat}}{M_{cat} \cdot \Gamma_{cat}} \right) \cdot \frac{1}{A_{geo}}$$

Here, A_{cat} and A_{geo} denote the catalytic and geometric surface area respectively, m_{cat} is the mass and M_{cat} is the molar mass of the corresponding noble metal, and Γ_{cat} is the surface site density. D is the noble metal dispersion derived from the CO-TPD results. Noble metal dispersion and $F_{cat/geo}$ for all samples are given in Table 3.

In Figure 6, the correlation between $F_{cat/geo}$ and the noble metal loading of the catalysts is shown. Regarding only the range of loading used in this study, a linear relationship is found with good agreement. Considering the physical constraints that no loading is equal to zero $F_{cat/geo}$ and higher loadings lead to saturation, a power function regression is more suitable. However, for very low platinum loading the particle size distribution shifts to lower particle diameters and structure sensitivity becomes more eminent. Now the correlations are only valid for catalysts pretreated with 10% water in air for 16 h at 700 °C, but further research addressed to varied conditions is in progress.

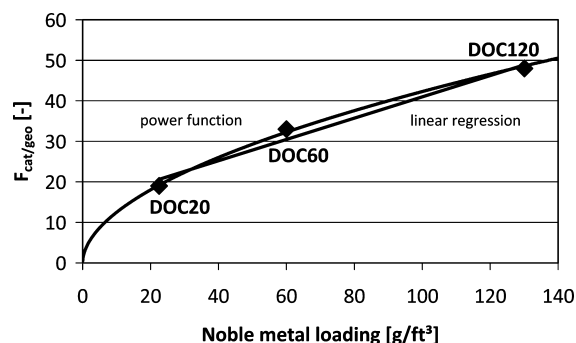


Figure 6. Correlation of $F_{cat/geo}$ and noble metal loading.

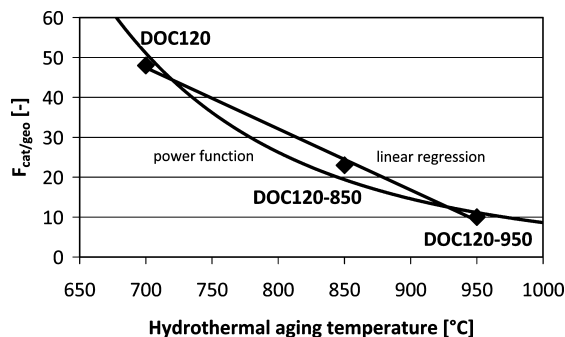


Figure 7. Correlation of $F_{cat/geo}$ and hydrothermal aging temperature.

For hydrothermal aging a similar linear correlation with $F_{cat/geo}$ can be generated for the temperature range used. Here the results (Figure 7) are fixed to a certain metal loading. Enhanced agreement is achieved by applying a power function that takes into account remaining activity for elevated temperatures. For temperatures that cause no deactivation, establishing a valid correlation is not feasible and a maximum for $F_{cat/geo}$ has to be defined.

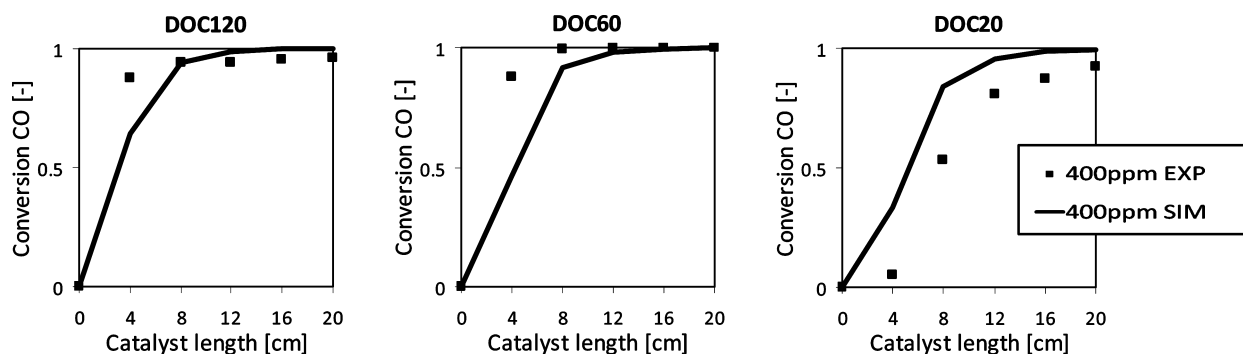


Figure 8. Axial profiles of CO conversion for catalysts with variation of noble metal loading at 120 °C: 400 ppm CO, 10% H₂O, 6.7% CO₂, and 12% O₂, balanced by N₂.

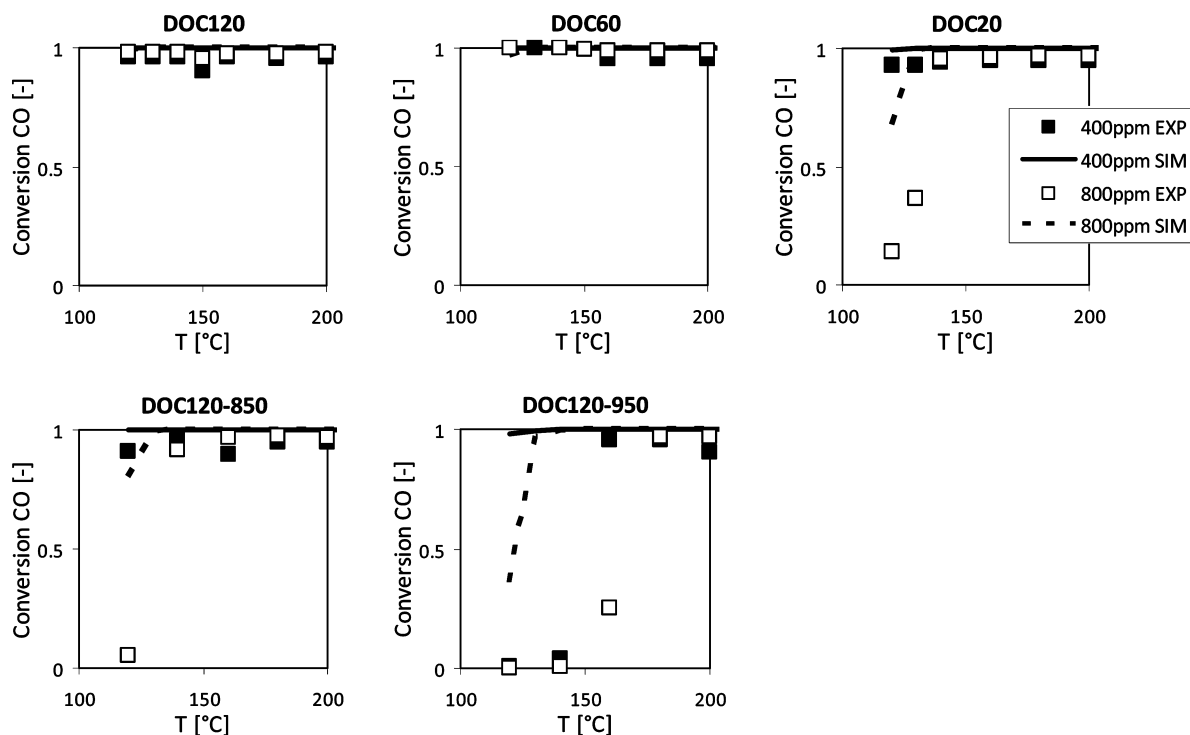


Figure 9. CO conversion determined behind the last catalyst slice as function of temperature for all catalyst samples: 400/800 ppm CO, 10% H₂O, 6.7% CO₂, and 12% O₂, balanced by N₂.

4.4. Catalytic Conversion of Pollutants. Isothermal flat bed reactor measurements with variation of CO, C₃H₆, and NO concentrations were used as reference. In all cases, 10% H₂O, 6.7% CO₂, and 12% O₂ are part of the synthetic exhaust gas, balanced by N₂. A very large number of cases was studied experimentally and numerically; only a few results are shown here demonstrating the effect of aging and metal loading variations.

4.4.1. CO Oxidation. CO as single pollutant with concentrations of 400 and 800 ppm were studied at temperatures between 120 and 200 °C. In Figure 8, the conversion of CO (400 ppm) is plotted along the flow direction in the catalyst. As the catalyst slices in the flat bed reactor have a length of 4 cm, gas compositions are obtained for 4-cm intervals. The model can predict the effect of the variation of catalyst loading on CO conversion well, taking only the active catalytic surface ($F_{cat/geo}$) as model parameter for the description of loading variations.

In Figure 9, the CO conversion reached behind the last catalyst slice for 400 and 800 ppm inlet CO concentration is shown for both variations of noble metal loading and hydrothermal aging temperature. As function of temperature, a pre-

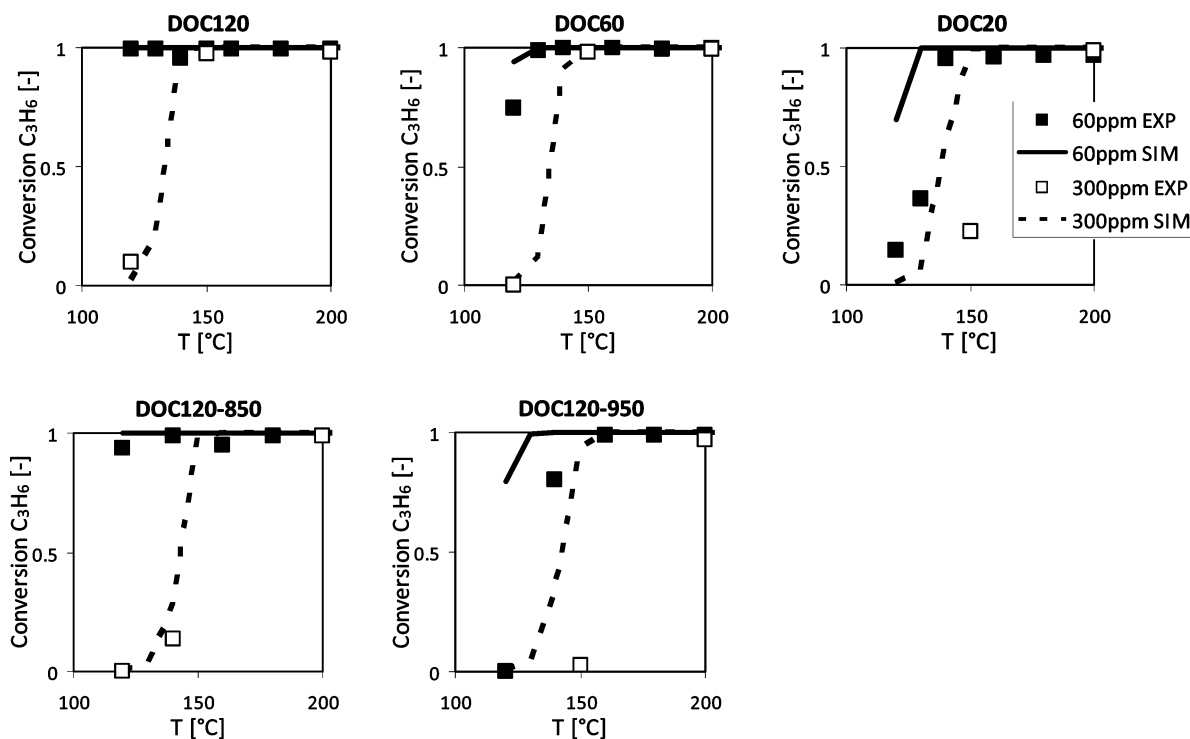


Figure 10. C₃H₆ conversion determined behind the last catalyst slice as function of temperature for all catalyst samples: 60/300 ppm C₃H₆, 10% H₂O, 6.7% CO₂, and 12% O₂, balanced by N₂.

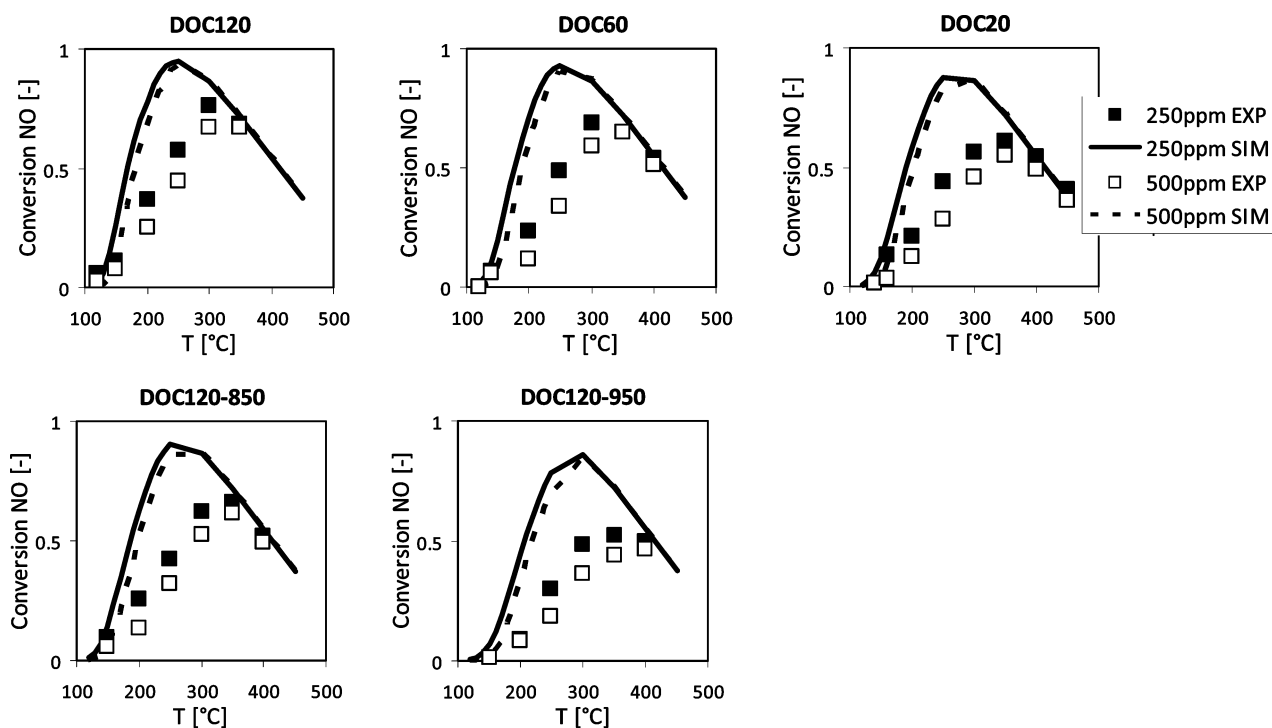


Figure 11. NO conversion determined behind the last catalyst slice as function of temperature for all catalyst samples: 250/500 ppm NO, 10% H₂O, 6.7% CO₂, and 12% O₂, balanced by N₂.

diction of the experimental results for all catalysts except DOC120-950 is achieved. For DOC120-950 the computed CO conversion leads to a higher activity than measured. Deactivation processes not apparent by catalyst characterization and probably caused by the harsh hydrothermal treatment may explain the deviations and reveal the limits of the model approach.

4.4.2. C₃H₆ Oxidation. Conversion of propylene as representative species of all reactive hydrocarbons in the exhaust gas is studied with 60 ppm and 300 ppm C₃H₆ concentration in

the feed. In Figure 10, C₃H₆ conversion, i.e., total oxidation toward CO₂ and H₂O is shown as function of temperature for all catalyst samples. Again, using F_{catgeo} only as model parameter can reproduce all experimentally observed trends. In contrast to the CO oxidation, the activity of DOC120-950 interpreted by the model approach is only slightly overestimated. Regarding DOC20 and DOC120-950, which exhibit nearly identical specific catalytic surface, the deviations between experiment and simulation are similar. For this reason, the C₃H₆

oxidation by DOC120-950 could not be affected by hydrothermal aging. Rather, the overpredicted conversion is caused by exceeding the extrapolation limits of the kinetic parameters optimized for DOC120.

4.4.3. NO Oxidation. Oxidation of NO to NO₂ is studied at inlet feed concentrations of 250 and 500 ppm. NO oxidation is limited by the thermodynamic equilibrium between NO and NO₂ above 350 °C, while NO conversion is kinetically controlled at lower temperatures. Using $F_{cat/geo}$ as the only model parameter and the rate coefficients optimized for DCO120, the model systematically overpredicts conversion in the temperature range between 200 and 300 °C (Figure 11). It is likely that this overprediction is caused by the fact that platinum oxide formation is not considered in the model. In literature, platinum oxide formation by NO₂ during NO oxidation has recently been discussed.^{15–17} Once platinum oxides (PtO and PtO₂) are formed at temperatures above 200 °C, a decrease in NO oxidation rates, i.e., the PtO_x catalyst is much less active than the reduced platinum catalyst. If the simulation results are restricted to temperatures aside catalyst deactivation, the model approach performs well for the kinetically and thermodynamically limited regime. Further investigations on platinum oxide formation are in progress.¹⁸

Summary

Several close-to-production platinum-based model DOCs with varying noble metal loadings and hydrothermal aging procedures are characterized in terms of specific platinum surface area and particle size as well as CO, C₃H₆, and NO oxidation behavior. Assuming no structure sensitive reactions, it is shown that, in principle, the catalytic active surface area determined by CO-TPD can serve as parameter to model the varying noble metal loading. It is not necessary to adapt any kinetic parameters in the original reaction mechanism. Concerning the effect of hydrothermal aging on conversion, the model approach predicts the effects qualitatively only with respect to increasing aging temperatures. The formation of platinum oxide by NO₂ is assumed to cause catalyst deactivation during NO oxidation, which is not considered in the mechanism yet.

By developing a reliable model for a platinum catalyst, a first step toward simulation of NSCs is achieved including effects of catalyst loading variations and hydrothermal aging. Considering the decrease of noble metal dispersion of hydrothermally aged catalysts, this model enables a prediction of conversion of exhaust gases in catalysts with reduced activity, once the general mechanism is established. The simulations can now support optimization of catalyst loadings, e.g., by considering a more economical non-uniform distribution along the channel axis.¹⁹ Catalyst stability can be enhanced by identifying the most sensitive components or reaction steps most affected by hydrothermal aging.

Acknowledgment

We thank Ulrich Nieken, Gerhart Eigenberger, and Karin Hauff (ICVT, University of Stuttgart) for sharing their kinetic

measurements. We gratefully acknowledge the financial support by the Forschungsvereinigung Verbrennungskraftmaschinen (FVV) e.V., and appreciate the efforts and kindness of Umicore AG&Co.KG for preparation and providing model catalysts.

Literature Cited

- (1) Epling, W. S.; Campbell, L. E.; Yezerets, A.; Currier, N. W.; Parks, J. E. Overview of the fundamental reactions and degradation mechanisms of NO_x storage/reduction catalysts. *Catal. Rev.-Sci. Eng.* **2004**, *46*, 163.
- (2) Roy, S.; Baiker, A. NO_x Storage-Reduction Catalysis: From Mechanism and Materials Properties to Storage-Reduction Performance. *Chem. Rev.* **2009**, *109*, 4054.
- (3) Koop, J.; Deutschmann, O. Detailed surface reaction mechanism for Pt-catalyzed abatement of automotive exhaust gases. *Appl. Catal., B* **2009**, *91*, 47.
- (4) Chatterjee, D.; Deutschmann, O.; Warnatz, J. Detailed surface reaction mechanism in a three-way catalyst. *Faraday Discuss.* **2001**, *119*, 371.
- (5) Foger, K.; Anderson, J. R. Temperature Programmed Desorption of Carbon-Monoxide Adsorbed on Supported Platinum Catalysts. *Appl. Surf. Sci.* **1979**, *2*, 335.
- (6) Schmeißer, V.; Perez, J.; Tuttlies, U.; Eigenberger, G. Experimental results concerning the role of Pt, Rh, Ba, Ce and Al₂O₃ on NO_x-storage catalyst behaviour. *Top. Catal.* **2007**, *42*, 15.
- (7) Deutschmann, O.; Tischer, S.; Kleditzsch, S.; Janardhanan, V. M.; Correa, C.; Chatterjee, D.; Mladenov, N.; Minh, H. D. DETCHEM Software package, version 2.2, www.detchem.com, Karlsruhe, 2008.
- (8) Mladenov, N.; Koop, J.; Tischer, S.; Deutschmann, O. Modeling of transport and chemistry in channel flows of automotive catalytic converters. *Chem. Eng. Sci.* **2010**, *65*, 812.
- (9) Ertl, G. Reactions at well-defined surfaces. *Surf. Sci.* **1994**, *300*, 742.
- (10) Maier, L.; Schädel, B.; Herera Delgado, K.; Tischer, S. Steam Reforming of Methane over Nickel: Development of a Multi-Step Surface Reaction Mechanism. *J. Phys. Chem.* 2010. submitted.
- (11) Eberhardt, M.; Riedel, R.; Gobel, U.; Theis, J.; Lox, E. S. Fundamental investigations of thermal aging phenomena of model NO_x storage systems. *Top. Catal.* **2004**, *30*, 135.
- (12) Wanke, S. E.; Flynn, P. C. Sintering of Supported Metal-Catalysts. *Catal. Rev.-Sci. Eng.* **1975**, *12*, 92.
- (13) Flynn, P.; Wanke, S. Model of Supported Metal Catalysts Sintering. 1. Development of Model. *J. Catal.* **1974**, *34*, 390.
- (14) Gracia, F.; Wolf, E. Non-isothermal dynamic Monte Carlo simulations of CO oxidation on Pt supported catalysts. *Chem. Eng. Sci.* **2004**, *59*, 4723.
- (15) Després, J.; Elsener, M.; Koebel, M.; Kröcher, O.; Schnyder, B.; Wokaun, A. Catalytic oxidation of nitrogen monoxide over Pt/SiO₂. *Appl. Catal., B* **2004**, *50*, 73.
- (16) Olsson, L.; Fridell, E. The Influence of Pt Oxide Formation and Pt Dispersion on the Reactions NO₂ ↔ NO + 0.5 O₂ over Pt/Al₂O₃ and Pt/BaO/Al₂O₃. *J. Catal.* **2002**, *210*, 340.
- (17) Hauptmann, W.; Votsmeier, M.; Gieshoff, J.; Drochner, A.; Vogel, H. Inverse hysteresis during the NO oxidation on Pt under lean conditions. *Appl. Catal., B* **2009**, *93*, 22.
- (18) Chan, D. Mechanismentwicklung für die Umsetzung von NO zu NO₂ über Platin. Master thesis, Department of Chemistry and Biosciences, Karlsruhe Institute of Technology (KIT), Karlsruhe, Germany, 2010.
- (19) Minh, H. D.; Bock, H. G.; Tischer, S.; Deutschmann, O. Optimization of Two-Dimensional Flows with Homogeneous and Heterogeneously Catalyzed Gas-Phase Reactions. *AIChE J.* **2008**, *54*, 2432.

Received for review March 7, 2010

Revised manuscript received June 7, 2010

Accepted June 10, 2010

IE100516J